AD-A133 517 CAVITATION INCEPTION OBSERVATIONS ON AXISYMMETRIC HEADFORMS WITH TURBULENCE STIMULATORS(U) DAVID W TAYLOR NAVAL SHIP RESEARCH AND DEVELOPMENT CENTER BET.. 1/1

UNCLASSIFIED T T HUANG ET AL. SEP 83 DTNSRCC-83/071 F/G 20/4 NL

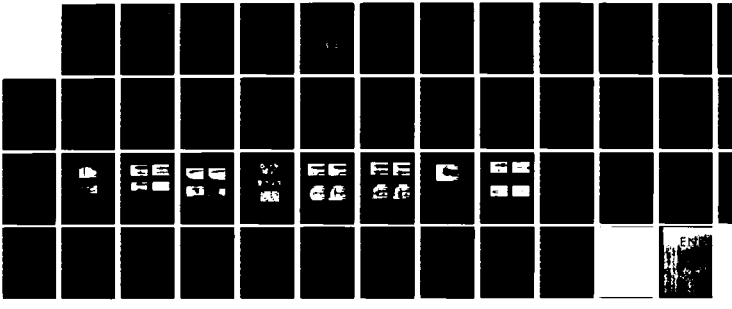

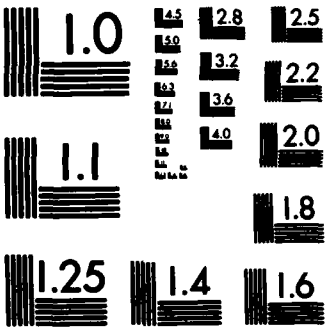

MICROCOPY RESOLUTION TEST CHART
NATIONAL BUREAU OF STANDARDS-1963-A

(12)

DAVID W. TAYLOR NAVAL SHIP RESEARCH AND DEVELOPMENT CENTER

Bethesda, Maryland 20084

DTNSRDC-83/071

AD-A133 517

CAVITATION INCEPTION OBSERVATIONS ON AXISYMMETRIC HEADFORMS WITH TURBULENCE STIMULATORS

DTIC FILE COPY

CAVITATION INCEPTION OBSERVATIONS ON AXISYMMETRIC HEADFORMS WITH TURBULENCE STIMULATORS

by

Thomas T. Huang
Garnell S. Belt
Nancy C. Groves

APPROVED FOR PUBLIC RELEASE: DISTRIBUTION UNLIMITED

SHIP PERFORMANCE DEPARTMENT
RESEARCH AND DEVELOPMENT REPORT

September 1983

DTNSRDC-83/071

MAJOR DTNSRDC ORGANIZATIONAL COMPONENTS

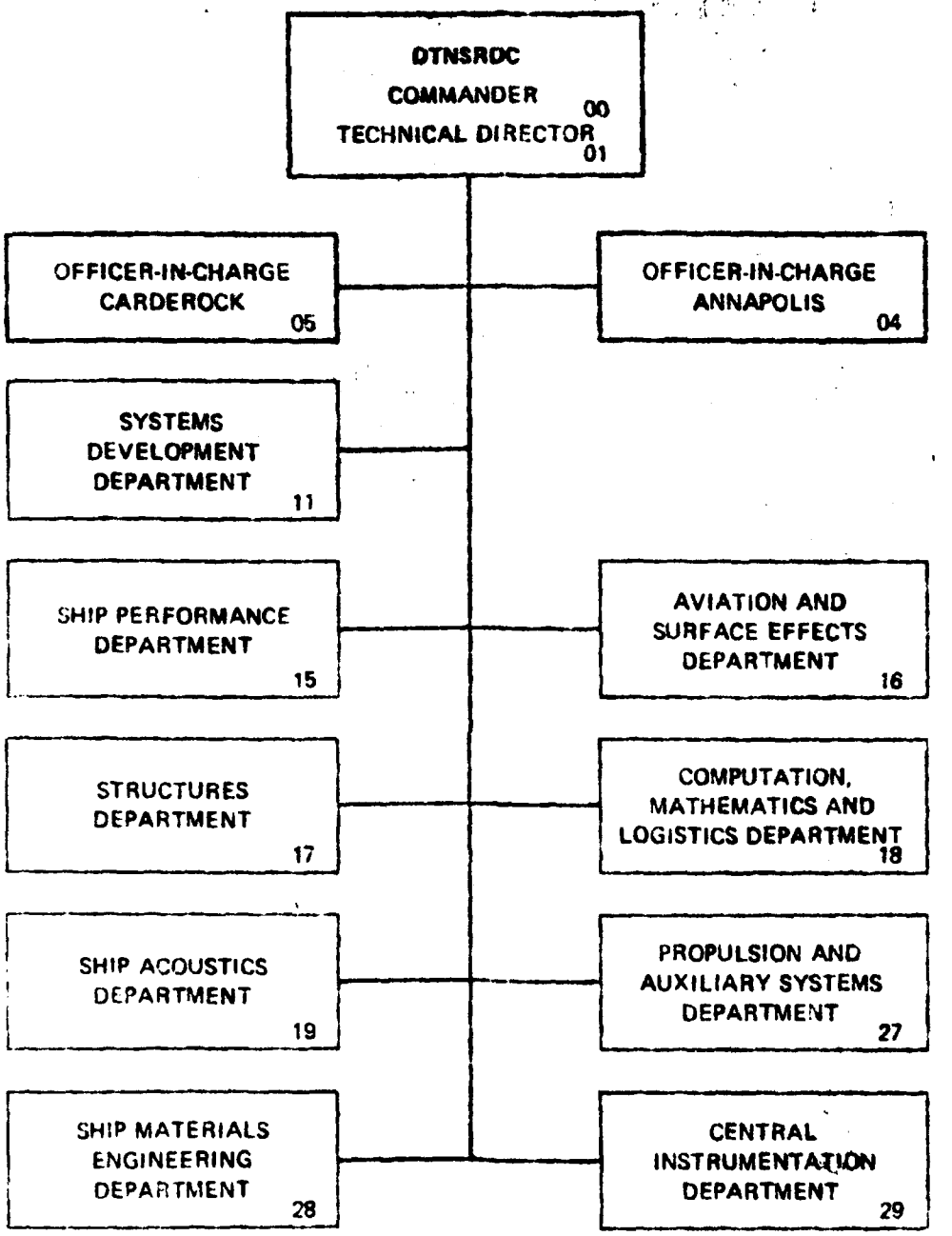

UNCLASSIFIED

SECURITY CLASSIFICATION OF THIS PAGE (When Data Entered)

REPORT DOCUMENTATION PAGE		READ INSTRUCTIONS BEFORE COMPLETING FORM
1. REPORT NUMBER DTNSRDC-83/071	2. GOVT ACCESSION NO. AD-A133517	3. RECIPIENT'S CATALOG NUMBER
4. TITLE (and Subtitle) CAVITATION INCEPTION OBSERVATIONS ON AXISYMMETRIC HEADFORMS WITH TURBULENCE STIMULATORS		5. TYPE OF REPORT & PERIOD COVERED Final 6. PERFORMING ORG. REPORT NUMBER
7. AUTHOR(s) Thomas T. Huang, Garnell S. Belt, and Nancy C. Groves		8. CONTRACT OR GRANT NUMBER(s)
9. PERFORMING ORGANIZATION NAME AND ADDRESS David W. Taylor Naval Ship Research and Development Center Bethesda, Maryland 20084		10. PROGRAM ELEMENT, PROJECT, TASK AREA & WORK UNIT NUMBERS Program Element 61153N Task Area SR0230101 Work Unit 1542-817
11. CONTROLLING OFFICE NAME AND ADDRESS Naval Sea Systems Command Code 05R24 Washington, D.C. 20362		12. REPORT DATE September 1983 13. NUMBER OF PAGES 49
14. MONITORING AGENCY NAME & ADDRESS(if different from Controlling Office)		15. SECURITY CLASS. (of this report) UNCLASSIFIED 15a. DECLASSIFICATION/DOWNGRADING SCHEDULE

16. DISTRIBUTION STATEMENT (of this Report)

APPROVED FOR PUBLIC RELEASE: DISTRIBUTION UNLIMITED

17. DISTRIBUTION STATEMENT (of the abstract entered in Block 20, if different from Report)

18. SUPPLEMENTARY NOTES

19. KEY WORDS (Continue on reverse side if necessary and identify by block number)

Cavitation Inception
Distributed Roughness
Isolated Roughness
Turbulence Stimulators

e to the Nth power

20. ABSTRACT (Continue on reverse side if necessary and identify by block number)

Cavitation inception observations were made in the DTNSRDC 36-inch water tunnel on three axisymmetric headforms with and without various turbulence stimulators installed. Direct measurements of transition, made on two of the headforms with and without distributed surface roughness, were found to correlate reasonably well with the computed spatial amplification factors, e^N

(Continued on reverse side)

DD FORM 1 JAN 73 1473 EDITION OF 1 NOV 65 IS OBSOLETE
S/N 0102-LF-014-6601

UNCLASSIFIED

SECURITY CLASSIFICATION OF THIS PAGE (When Data Entered)

(Block 20 continued)

with $7 \leq N \leq 10$. The computed e^N factors were then used to estimate transition at other test conditions (without direct transition measurements). The predicted transition locations on all three smooth headforms occur at positions considerably aft of the minimum pressure locations. The three smooth headforms have different types of incipient cavitation--small band, transient spot, traveling bubble, and attached spot. The measured cavitation inception numbers for those cases are all significantly smaller than the computed negative values of the minimum pressure coefficient, $-C_{p_{min}}$. The predicted transition locations on the three headforms with densely- and loosely-packed 60-μm distributed roughness occur a considerable distance upstream of the minimum pressure locations. Therefore, the flows over all three headforms with distributed roughness are turbulent at the $C_{p_{min}}$ locations for the Reynolds numbers tested. Under this condition, the measured cavitation inception numbers are found to approximate well the values of $-C_{p_{min}}$. The incipient cavitation is in the form of attached small bubble lines evenly distributed around the minimum pressure locations. The measured cavitation inception numbers for the three headforms with an isolated roughness band located upstream of the minimum pressure locations are found to approximate the computed values of $-C_{p_{min}}$ when the roughness Reynolds number ($R_K = u_K K/\nu$) is equal to or greater than 600 and to be smaller than the values of $-C_{p_{min}}$ when the value of R_K is less than 600. The incipient cavitation observed is attached patch type cavitation occurring in the vicinity of the minimum pressure locations.

TABLE OF CONTENTS

	Page
LIST OF FIGURES	iv
LIST OF TABLES	iv
NOTATION	v
ABSTRACT	1
ADMINISTRATIVE INFORMATION	1
INTRODUCTION	2
PREVIOUS RELEVANT RESEARCH ON CAVITATION INCEPTION ON BODIES USING TURBULENT STIMULATORS	4
GEOMETRY FOR THREE SMOOTH HEADFORMS	7
CAVITATION EXPERIMENTS	7
CAVITATION INCEPTION OBSERVATIONS ON THE SMOOTH HEADFORMS	8
TURBULENCE STIMULATORS	9
CAVITATION INCEPTION OBSERVATIONS ON HEADFORMS WITH TURBULENCE STIMULATORS	10
CORRELATION OF MEASURED CAVITATION INCEPTION WITH COMPUTED BOUNDARY-LAYER CHARACTERISTICS	12
CORRELATION FOR THREE SMOOTH HEADFORMS	14
CORRELATION FOR THREE HEADFORMS WITH DISTRIBUTED ROUGHNESS	16
CORRELATION FOR THREE HEADFORMS WITH ISOLATED ROUGHNESS BANDS	16
CONCLUSIONS	17
APPENDIX - CORRELATION FOR SCHIEBE MODEL	35
REFERENCES	37

LIST OF FIGURES

Page

1 - Surface Profiles and Pressure Coefficients of Three Headforms 19

2 - Small Band Cavitation Inception Occurring at a Laminar Separation Location on the Smooth S-1 Headform 20

3 - Three Sizes of Large Transient Spots at Laminar Separation on Smooth S-2 Headforms 21

4 - Two Types of Cavitation Inception on the Smooth Headform T-6. 22

5 - Distributed Roughness (Amplified × 110) 23

6 - Cavitation Inception on Headform S-1 with Boundary-Layer Turbulence Stimulators. 24

7 - Cavitation Inception on Headform S-2 with Boundary-Layer Turbulence Stimulators. 27

LIST OF TABLES

1 - Measured Cavitation Inception on Smooth Headforms with Laminar Separation. 28

2 - Measured Cavitation Inception on Smooth Headform T-6 with Natural Transition 29

3 - Measured Cavitation Inception on Headform S-1 Having Various Boundary-Layer Turbulence Stimulators 30

4 - Measured Cavitation Inception on Headform S-2 Having Various Boundary-Layer Turbulence Stimulators 31

5 - Measured Cavitation Inception on Headform T-6 Having Various Boundary-Layer Turbulence Stimulators 33

6 - Transition Predictions for Schiebe Model ($-C_{pmin}$=0.75) with and without Distributed Roughness. 36

NOTATION

A		Cumulated spatial amplification ratio of a disturbance in the boundary layer to its amplitude at point of neutral stability
A^+		Threshold Reynolds number, assumed to equal 40
A_s		A at the position of laminar boundary-layer separation
C_p		Pressure coefficient given by $(P-P_o)/(1/2\rho U_o^2)$
C_{pmin}		Minimum value of C_p
C_{ps}		C_p at the position of laminar boundary-layer separation
C_{ptr}		C_p at the location of transition in the laminar boundary-layer
D		Diameter of the axisymmetric headform
K		$3K_s$, for distributed roughness about the average value of the maximum roughness depth in a single measuring length of 1 cm
	or	*Average vertical distance between the tip of the largest roughness* in a circumferential distance of 1 cm and the smooth surface at the leading edge of the isolated stimulator
K_s		Measured rms value of the roughness heights
P		Local static pressure on the headform
P_o		Free-stream tunnel static pressure
P_v		Vapor pressure of water at its bulk temperature
R_D		Reynolds number given by $U_o D/\nu$
$R_{D_{crit}}$		Critical Reynolds number at which transition takes place at the position of laminar boundary-layer separation
R_K		$\frac{u_K K}{\nu}$, the roughness Reynolds number
U_o		Free-stream tunnel velocity

u_K	Local streamwise velocity component evaluated at the roughness height, K
X	Axial distance from the stagnation point
X_s	Axial distance from the stagnation point to the laminar separation point
X_{tr}	Axial distance from the stagnation point to the transition location
Y	Radial distance measured from the X-axis of the headform
y	Distance along the surface normal
α/α_o	Dissolved gas content in terms of percent of saturation at 21°C water temperature and atmospheric pressure
α/α_{TS}	Dissolved gas content in terms of percent saturation at test section water temperature and pressure
β_1	A constant, set equal to 1.0, in the momentum diffusivity term
ε_m	Momentum diffusivity term, (Equation (3))
ε_{max}	Amplitude of the momentum diffusivity at the wall
μ	Molecular viscosity
μ_t	$\mu + \rho\varepsilon_m$, roughness molecular viscosity
ν	Kinematic viscosity of water
ρ	Mass density of water
σ	Cavitation number given by $(P-P_v)/(1/2\rho U_o^2)$
σ_i	Incipient cavitation number

ABSTRACT

Cavitation inception observations were made in the DTNSRDC 36-inch water tunnel on three axisymmetric headforms with and without various turbulence stimulators installed. Direct measurements of transition, made on two of the headforms with and without distributed surface roughness, were found to correlate reasonably well with the computed spatial amplification factors, e^N with $7 \leq N \leq 10$. The computed e^N factors were then used to estimate transition at other test conditions (without direct transition measurements). The predicted transition locations on all three smooth headforms occur at positions considerably aft of the minimum pressure locations. The three smooth headforms have different types of incipient cavitation--small band, transient spot, traveling bubble, and attached spot. The measured cavitation inception numbers for those cases are all significantly smaller than the computed negative values of the minimum pressure coefficient, $-C_{pmin}$. The predicted transition locations on the three headforms with densely- and loosely-packed 60-μm distributed roughness occur a considerable distance upstream of the minimum pressure locations. Therefore, the flows over all three headforms with distributed roughness are turbulent at the C_{pmin} locations for the Reynolds numbers tested. Under this condition, the measured cavitation inception numbers are found to approximate well the values of $-C_{pmin}$. The incipient cavitation is in the form of attached small bubble lines evenly distributed around the minimum pressure locations. The measured cavitation inception numbers for the three headforms with an isolated roughness band located upstream of the minmum pressure locations are found to approximate the computed values of $-C_{pmin}$ when the roughness Reynolds number ($R_K=u_K K/\nu$) is equal to or greater than 600 and to be smaller than the values of $-C_{pmin}$ when the value of R_K is less than 600. The incipient cavitation observed is attached patch type cavitation occurring in the vicinity of the minimum pressure locations.

ADMINISTRATIVE INFORMATION

This work was funded by the David W. Taylor Naval Ship Research and Development Center, General Hydromechanics Research Program, Program Element 61153N, Task Area SR0230101, and performed under Work Unit 1542-817.

INTRODUCTION

Inception of cavitation in liquids is the condition under which cavitation is first detected, either visually or acoustically, with a simple measuring device. The simple assumption that equilibrium conditions are reached instantaneously and that the cavitation inception occurs immediately when the static pressure reaches the vapor pressure is often made in engineering predictions of cavitation inception. This assumption is probably valid for most full-scale bodies. However, the Reynolds number at model scale is one or two orders of magnitude smaller than the prototype value. The measured cavitation indices σ_i on small smooth models are generally significantly smaller than the negative value of the minimum pressure coefficient, $-C_{pmin}$ (see Huang,[1*] Arakeri and Acosta,[2] Holl and Carroll,[3] Van der Meulen,[4] and Van der Meulen and Ye[5]). The boundary layers on the smooth models are usually laminar at the location of the minimum static pressure and remain laminar for a considerable length downstream. In contrast, transition from laminar to turbulent flow is most likely to take place upstream of a prototype minimum pressure location. Extensive reviews of the viscous effects on cavitation inception have been made by Acosta and Parkin[6,7] and by Acosta.[8] Detailed numerical evaluations of the influence of viscous effects on model and full-scale cavitation inception correlation have been made by Huang and Peterson.[9] Prediction techniques and a large amount of data covering the scale effects on various types of cavitation have also been presented by Billet and Holl.[10] The viscous characteristics of the flow regime (whether laminar, laminar separated, transitional, or fully turbulent), at and upstream of the cavitation-prone minimum pressure location, play extremely important roles in the small model cavitation inception process, and the differences in flow regimes between model and full scale are the major sources of the so-called "scale effects" of cavitation inception.

Another controlling factor in cavitation inception is the size and population of the free-stream microscopic air bubbles in the flow facility. Large exposed free surface areas in the facility may result in an over-deaerated fluid during prolonged low pressure operation. The resulting lack of microbubbles has been found to prevent the proper development of cavitation inception. Artificial seeding of the fluid with microbubbles has been found to stimulate cavitation inception, by

---

*A complete listing of references is given on page 37.

Albrecht and Bjorheden[11] in the Ka Me Wa (KMW) Marine Laboratory free-surface cavitation tunnel, and by Noordzij[12] in the Netherland Ship Model Basin depressurized towing tank. Increasing microbubble population in most closed-loop water tunnels has been found to promote traveling bubble inception (Gates and Acosta,[13] and Ling et al.[14]). In some cases,[13] free-stream microbubbles serve to trip the boundary layer and almost eliminate laminar separation on the model. However, the effects of gross gas content on the attached types of cavitation (bubble-ring, band, transient spots, or fixed patch) are, in general, rather small.[1,3]

A high free-stream turbulence level is known to promote an early boundary-layer transition and, in certain conditions, early transition can lead to complete elimination of laminar separation.[13] It is expected that the effect of free-stream turbulence on cavitation inception becomes important when the turbulence level can cause significant change in transition and/or laminar separation.

Neither a high free-stream turbulence level nor a microbubble seeding is a reliable and practical technique for stimulating boundary-layer transition on models in cavitation tunnels. The magnitude of turbulence levels in water tunnels varies from 0.05%-0.2% (good quality) to 0.2%-1% (normal) and up to a maximum of 2% (in some tunnels). If a tunnel has a turbulence level higher than 2%, the result is usually a significant degrading of the tunnel's capability and flow quality to the point where cavitation experiments cannot be performed. To seed microbubbles uniformly across the test section without generating excessive vortices is also not a simple task. Furthermore, a proper seeding technique to assure model-to-full-scale correlation is not yet available and would be difficult to develop.

Scale effect prediction techniques[9,10] may only be used to estimate the trend and the order of magnitude of the scale effects of cavitation inception and are not sufficiently accurate to give quantitative results. In addition, the prediction techniques require accurate knowledge of the pressure distribution. Such detailed information is often not available for three-dimensional bodies and propellers.

Reliable and practical techniques to eliminate scale effects in the experimental procedure would be of great value to cavitation model testing in water tunnels. One promising technique is the use of a boundary-layer turbulence

stimulator consisting of a microscopic distributed roughness from the leading edges of the propellers and hydrofoils, or the noses of bodies to an appropriate location upstream or downstream of the minimum pressure location. In the following, recent research relative to these techniques is reviewed. Further research to perfect the techniques for model applications will also be reviewed.

PREVIOUS RELEVANT RESEARCH ON CAVITATION INCEPTION ON BODIES USING TURBULENT STIMULATORS

A boundary-layer tripping technique using a strip of 60 μm (for between approximately 53 and 62 μm) Carborundum irregular particles about 1 mm from the leading edges of propeller blades has been developed by Kuiper[15-18] to stimulate the boundary layer on a propeller model and thus to reduce viscous effects on propeller cavitation. A paint flow visualization technique showed the roughness to be quite effective in producing turbulent boundary layers on almost the entire chord length of the blades. Furthermore, Kuiper[16-18] concluded that the microbubble nuclei generated by the leading edge roughness apparently promoted the inception of bubble cavitation further downstream. Thus, the application of leading edge roughness is capable of not only reducing viscous effects, but also providing needed nuclei. However, the leading edge roughnesses could also produce an undesired pressure disturbance near the minimum pressure location that might cause early cavitation on the roughness elements.

Propeller cavitation research is one of the most important areas of cavitation research. However, the pressure distributions and the three-dimensional boundary-layer properties of the propellers are often not available or, if available, not accurately determined. Therefore, basic understanding of the effects of the leading-edge roughness tripping on cavitation is difficult to obtain from propeller model tests. More definitive experiments must be made on simpler models such as axisymmetric headforms or hydrofoils. For such models, accurate information on the pressure distributions and boundary-layer properties are relatively easy to obtain. The cavitation results obtained with such models are given next.

Billet and Holl[19] used distributed roughnesses having mean diameters of 30 μm and 66 μm on the nose, but upstream of the minimum pressure locations, of two small Schiebe headforms (D=25.4 and 50.8 mm). The roughnesses were distributed from the stagnation point extending aft to a local diameter D_r. The values of D_r/D

investigated were 0.5 and 0.7. The 66 μm distributed roughness, with $D_r/D = 0.5$, had no influence on cavitation for either body. This roughness extent may not have been sufficient to trip the boundary layer and to generate small microbubbles. However, for the larger value of $D_r/D = 0.7$ with 30 μm particles, fixed-patch cavitation, having a patch of cavitation attached to the surface near the minimum pressure location, was observed. Cavitation was not observed on the roughness elements. The incipient cavitation number σ_i for traveling-bubble and fixed-patch cavitation for both bodies occurred at higher values than did the similar type of cavitation for the bodies without added roughness. It is important to note that the effects on cavitation of the distributed roughness on the nose of the model depend upon the extent of roughness upstream of the C_{pmin} location; one case seems to trip the boundary layer and the other is not effective at all. One can match σ_i of the model and prototype by employing a trial and error process of adding roughness; but to do this, one must know σ_i of the prototype.

Experimental investigations were conducted by Van der Meulen and Ye[5] on a slightly tapered NACA 4412 hydrofoil at an angle of attack of 2 deg with $-C_{pmin} = 1.105$ at $x/C = 0.28$. The experimental series comprised measurements of the pressure distribution, and on-line holographic recordings of: 1. the boundary layer flow, 2. traveling-bubble cavitation, and 3. bubble population. Two configurations were tested where bubbles were generated by a cavitating wire (1 mm or 0.25 mm diameter) ahead of the foil. The influence of artificial roughness was studied for five different configurations: 0.65-μm distributed roughness, 50-μm trip wire at $x/C = 0.05$, 60-μm trip of sand roughness at $x/C = 0.0054 - 0.0100$, narrow band (suction side $x/C=0-0.05$ and pressure side $x/C=0-0.015$) of 30-μm sand roughness, and wide band (suction side $x/C=0-0.072$ and pressure side $x/C=0-0.036$) of 30-μm sand roughness. Without the application of roughness, the boundary layer was laminar up to a midchord position where transition to turbulence (at low speeds laminar flow separated at midchord) occurred. The types of cavitation observed were traveling-bubble or transient-spot cavitation. When roughness was applied, early transition to turbulence occurred, but this had no effect on the inception or appearance of traveling-bubble cavitation. However, when nuclei generation ahead of the foil was applied or when the roughness elements on the foil were cavitating, the type of

cavitation changed to attached bubble cavitation. The measured incipient cavitation number σ_i on the foil having a leading-edge roughness band trip was found to simulate very closely the value of $-C_{pmin} = 1.105$, whereas the measured value of σ_i on the smooth foil is 0.99. The scale effect on this model was only moderate. The measured values of σ_i were 1.24 and 1.20 when the 1 mm and 0.25 mm diameter cavitating wires were upstream of the foil, respectively. Vortices generated by the wires caused premature cavitation, which must be avoided for a successful experiment. The average roughness of 0.65 μm for the distributed roughness was, unfortunately, too small to have any significant effect on cavitation inception.

A new foil section (YS-920) was designed by Shen and Eppler[20] to have a wider cavitation-free bucket at the full-scale Reynolds number than that of the NACA 66 (MOD) section. A natural transition to turbulence near the leading edge will occur at the full-scale Reynolds number. However, at model scale, the boundary layer will be laminar. A uniformly distributed roughness, consisting of spherical glass beads of 90 μm diameter covering the first 1.5% of the chord length on both the upper and lower surfaces, was used to simulate the high Reynolds number cavitation phenomenon.[21] The computed cavitation-free boundaries of the two foils at various angles of attack (based on the assumption that $\sigma_i = -C_{pmin}$ at full scale) agreed very well with the measured boundaries of the two foils using leading edge roughness but did not agree with the measured boundaries of the smooth foils.[21] In this experiment,[21] a slight (less than 5%) reduction of lift curve slope, a 0.25 deg increase in zero-lift angle, and a 40-50% increase in section drag coefficient were caused by the leading edge roughness. Shen[21] also found that the termination of roughness at $x/C = 0.015$ caused a pressure disturbance there and that, at an angle of attack having C_{pmin} located at about $x/C = 0.015$, the measured incipient cavitation number was slightly larger than the value of C_{pmin}. Similar to the results of Van der Meulen and Ye,[5] Shen[21] found that the scale effects on the midchord cavitation inception are effectively eliminated by using leading-edge roughness.

In order to gain further insight into the physics of cavitation inception on bodies with turbulence stimulators, and to obtain hydrodynamic parameters for selecting effective turbulence stimulators to reduce scale effects on cavitation inception, three axisymmetric headforms with distributed roughness and isolated strip roughness were tested in the DTNSRDC 36-in. water tunnel. A brief summary of this work is reported in the following sections.

GEOMETRY FOR THREE SMOOTH HEADFORMS

Two axisymmetric headforms having laminar separation and a third having natural flow transition were selected to investigate the effects of various boundary-layer turbulence stimulators on cavitation inception. Cavitation inception observations on the three smooth headforms were made by Huang.[1] The headform designated T-6 has natural transition without any possibility of laminar separation. The other two headforms, designated as S-1 (hemispheric nose) and S-2, exhibit laminar separation as a result of severe adverse pressure gradients. Use of fluorescent oil-film visualization techniques in the water tunnel verified the existence of laminar separation at the predicted locations.[1] The body contours and the distributions of the potential-flow pressure coefficients of the three headforms are shown in Figure 1. The Headforms T-6 and S-1 have the same maximum diameter (D=10.2 cm). Three scales of Headform S-2 were constructed with maximum diameters of D = 10.2 cm, 7.63 cm, and 2.54 cm. All the headforms were constructed of plexiglass to avoid corrosion and the surface finish was kept at 0.4 μm.

CAVITATION EXPERIMENTS

The experiments were carried out in the DTNSRDC 36-in. Variable Pressure Water Tunnel (VPWT) with a closed-jet test section. A cylindrical resorber 7.62 m in diameter and 21.3 m in height is built into the circuit to reduce the free-air content of the water. The tunnel is also equipped with a deaeration system which can be used to reduce the air content of the water. Total air content was measured by a standard Van Slyke apparatus. All cavitation measurements were made with a dissolved air content of 9 parts per million by weight, corresponding to 40% of saturation at 21°C water temperature at atmospheric pressure. No quantitative measurements of free-gas bubble distribution were made in the present experiment.

The headforms were attached to the housing of the propeller shaft located at the centerline of the test section and were illuminated by an EG&G Xenon Stroboscope (Model LS 148). The system allowed the visual observation of cavitation bubbles. Traveling-bubble cavitation inception is defined in this report as the onset of detectable cavitation events which occur about once per second. Transient spot, band, and attached cavitation inceptions usually occur very suddenly and are quite

repeatable. Therefore, their inception values are rather easy to obtain. Most of the cavitation events on the three headforms were recorded photographically by using Polaroid High-Speed Type-52 film or Kodak High-Speed Ektachrome 32-mm film. In addition, high-speed motion pictures (6500 frames per second) were taken by a Red Lake Hycam 16-mm camera.

Incipient cavitation numbers were determined by slowly lowering the tunnel pressure at constant tunnel velocity until cavitation events occurred. The cavitation number, σ, is given by

$$\sigma = \frac{P_o - P_v}{1/2\ \rho U_o^2} \tag{1}$$

where P_v = vapor pressure of the water

P_o = static pressure at the centerline of the test section

ρ = mass density of water

U_o = tunnel velocity

The incipient cavitation number is denoted by σ_i.

CAVITATION INCEPTION OBSERVATIONS ON THE SMOOTH HEADFORMS

The initial cavitation inception observations on the smooth headforms were reported by Huang.[1] The repeated observations during the present experiments show no discrepancy with the initial observations.

Figure 2 shows band cavitation with small parallel bubble lines distributed evenly at the laminar separation location on the smooth hemispheric headform S-1 at $\sigma_i = 0.61$. In Figure 3, large transient attached spot cavitation appears and disappears randomly on the smooth Headform S-2 at $\sigma_i = 0.30$ for the two large (D=10.2 cm and 7.63 cm) models and at $\sigma_i = 0.23$ for the small (D=2.54 cm) model. Cavitation inception on both Headforms S-1 and S-2 was found to occur near the location of laminar separation as detected by fluorescent oil-film visualization techniques (Figures 2 and 3). The Reynolds number at which natural transition first appears at the laminar separation location is designated as the critical Reynolds number, $R_{D_{crit}}$, and is given in Table 1.

Two types of cavitation inception on the Headform T-6, traveling bubble at $\sigma_i = 0.33$ and attached patch at $\sigma_i = 0.23$, are shown in Figure 4.

A summary of the measured cavitation inception data is given in Table 1 for Headforms S-1 and S-2 and in Table 2 for Headform T-6. As shown in Table 1, the measured incipient cavitation numbers for attached cavitation on the S-1 model and transient cavitation on the two larger S-2 models were found to be equal to the negative value of the static pressure coefficient, $\sigma_i = -C_{ps}$, at the separation locations. However, attached patch cavitation inception numbers on the small S-2 model were found to be less than $-C_{ps}$. According to the criterion given in Reference 9, the separation bubbles on this small S-2 model are long bubbles whereas those on the two large S-2 models and the S-1 model are short bubbles. The locations of patch cavitation on the T-6 model were found to be in the transition region, and the measured values of σ_i for the attached patch cavitation were found to be approximately equal to the negative value of the static pressure coefficient at transition, $\sigma_i \cong -C_{ptr}$. The values of σ_i for the traveling bubble cavitation of T-6 were found to vary between the negative value of the minimum static pressure coefficient $-C_{pmin}$ and C_{ptr} (Table 2).

The effect of air content was found to be significant only for the traveling bubble (T-6) cavitation and insignificant for the band (S-1), the transient (S-2), and the attached patch (T-6) types of cavitation. Therefore, a constant air content of 40% saturation was selected for this experiment.

It is important to note that the measured incipient cavitation numbers of the three smooth headforms tested in the DTNSRDC 36-in. water tunnel were significantly smaller than the values of $-C_{pmin}$. The boundary layers were certain to be laminar at the C_{pmin} location for all three smooth headforms.

TURBULENCE STIMULATORS

Three types of turbulence stimulators were used. The first type was a single band of roughness, 2.5 mm wide with 30-μm or 60-μm particles distributed evenly on the band. The second type consisted of densely packed particles of distributed roughness that started at the stagnation point and extended downstream of the C_{pmin} location. The same 60-μm Carborundum irregular particles used by Kuiper[15-18] and the 90-μm spherical glass beads used by Shen[20] were used to produce the distributed

roughnesses. In addition, some of the headforms were tested with a third type of roughness where the roughness particles were distributed but were not so densely packed. The difference between the densley and loosely packed distributed roughness is shown in Figure 5. The rms values of the roughness height as measured by a roughness meter (Perthometer Model C5D) are 15 μm and 10 μm for the densely and loosely packed distributed roughness, respectively.

The objectives of the roughness experiments were to find the minimum stimulator height necessary to cause transition to a fully turbulent boundary layer upstream of the minimum pressure location, to observe cavitation inception under this condition, to develop semiempirical relationships for transition prediction by various distributed and isolated turbulence stimulators and to identify the maximum stimulator height that does not promote premature and excessive cavitation.

CAVITATION INCEPTION OBSERVATIONS ON HEADFORMS WITH TURBULENCE STIMULATORS

Cavitation inception observations were made on the three headforms with various combinations of turbulence stimulators. The variation of the observed cavitation inception within the limited range of Reynolds numbers tested was found to be small. Therefore, cavitation inception data were obtained at only two values of Reynolds number for most of the headforms. In order to reduce water tunnel testing time, two different turbulence stimulators were applied on the upper and lower halves of the same headform during one experiment.

On hemispheric Headform S-1, three types of turbulence stimulators were used: 1. densely packed; 2. loosely packed 60-μm distributed roughness, both extending a considerable distance aft of the minimum pressure location; and 3. boundary-layer tripping bands (2.5-mm wide and 0.03-mm high) located at x/D of either 0.15 or 0.20. Cavitation inception observations on Headform S-1 with the three types of turbulence stimulators are shown in Figure 6. Attached small cavitating bubble lines evenly distributed around the C_{pmin} location were observed on the S-1 model with the two distributed roughnesses (Figures 6c, 6d, and 6g). The measured cavitation inception numbers vary from 0.77 to 0.79 (σ_i=0.78±0.01), which is approximately equal to the $-C_{pmin}$ value of 0.78. As shown in Figures 6h and 6i, large attached patch cavitation was observed on Headform S-1 with the boundary-layer tripping band

(located at both x/D=0.15 and 0.20). The measured cavitation inception numbers are 0.70 for the two band locations and are slightly smaller than the $-C_{pmin}$ value. The leading edges of the cavitation patches were located at a small distance downstream of the C_{pmin} location.

A densely packed 60-μm distributed roughness and a boundary-layer tripping band (4-mm wide and 0.06-mm high) located at x/D = 0.125 were used on the 10.2-cm Headform S-2 (Figure 7a). Cavitation inception on the distributed roughness surface was in the form of attached small cavitating bubble lines evenly distributed around the C_{pmin} location, whereas cavitation inception downstream of the tripping band was in the form of attached cavitating spots at the C_{pmin} location. The measured cavitation numbers for the two cases are $\sigma_i = 0.42 \pm 0.01$, which is again very close to the $-C_{pmin}$ value of 0.41. The three types of turbulence stimulators used on the small (D=2.54 cm) S-2 Headform were: 1. densely packed 60-μm distributed roughness (Figure 7b), 2. evenly packed 90-μm spherical glass beads (Figure 7c), and 3. a boundary layer tripping band (1.3-mm wide and 0.04-mm high) located at x/D = 0.25 (Figure 7d). The measured cavitation inception numbers for the distributed roughness are $\sigma_i = 0.42 \pm 0.02$. Again, the measured value of σ_i is very close to the $-C_{pmin}$ value of 0.41 and is located at the C_{pmin} location. The measured cavitation inception number downstream of the tripping band is $\sigma_i = 0.38$, which is slightly smaller than the $-C_{pmin}$ value.

The two types of turbulence stimulators used on Headform T-6 were: 1. densely packed 60-μm distributed roughness, and 2. a boundary-layer tripping band (2.5-mm wide and 0.03-mm high) located at x/D = 0.125. Cavitation inception in the form of attached cavitating bubble lines evenly distributed around the C_{pmin} location was observed on Headform T-6 with the densely packed distributed roughness. The measured cavitation inception number is 0.42 which again is very close to the $-C_{pmin}$ value of 0.43. Large attached cavitation patches downstream of the tripping band were observed on Headform T-6 with the isolated stimulation ring. The measured cavitation number is slightly smaller than the $-C_{pmin}$ value.

The measured cavitation inception indices for the three headforms with various turbulence stimulators are tabulated in Tables 3 through 5. For all of the headforms with densely packed 60-μm distributed roughness, cavitation inception was

observed at the C_{pmin} location and the measured cavitation inception numbers were found to be very close to the $-C_{pmin}$ values ($\sigma_i=-C_{pmin} \pm 0.02$). However, for headforms with an isolated ring of roughness, attached cavitation inception numbers were found to be slightly smaller than the $-C_{pmin}$ values except for the large (D=10.2 cm) Headform S-2 ($\sigma_i=-C_{pmin}$ in Table 4a). In the following section, the measured data given in Tables 3 through 5 will be correlated with computed boundary-layer characteristics.

CORRELATION OF MEASURED CAVITATION INCEPTION WITH COMPUTED BOUNDARY-LAYER CHARACTERISTICS

The laminar boundary layer on a small smooth model is quite stable from the stagnation point up to the location of C_{pmin}. Further downstream, the flow may or may not be separated depending upon the magnitude of the adverse pressure gradient. For a body having laminar separation, the Reynolds number at which natural flow transition first appears upstream of the laminar separation position is designated as the critical Reynolds number,[22] $R_{D_{crit}}$. Flows for which the Reynolds number is smaller or larger than $R_{D_{crit}}$ are called "subcritical" and "supercritical," respectively.[22] Use of fluorescent oil-film visualization on Headforms S-1 and S-2 in the 36-in. water tunnel verified the existence of laminar separation at the predicted locations[1] (Figures 2a and 3a). The Smith[23] spatial amplification factor has often been chosen as a simple yardstick to correlate the instability characteristics of the boundary layers with the various measured stages of transition. Satisfactory correlation between the computed amplification factors and measured transition processes on smooth bodies has been obtained by Huang[1] and Arakeri[24] in water tunnels; by Huang and Hannan,[25] and Huang[26] in a wind tunnel; and by Power[27] in the towing basin. Similar transition correlation techniques for bodies with distributed roughness will be developed in the following.

Distributed surface roughness is known to promote the early onset of boundary layer transition. Kosecoff et al.[28] developed an analytical model to simulate the effects of distributed surface roughness on transition. Merkle et al.[29] incorporated the Kosecoff analytical model into a computer program.

The primary effects of the distributed surface roughness are assumed to be distortions of the mean velocity profiles in a laminar boundary layer from their smooth-wall shapes. A momentum diffusivity term ε_m is added to the molecular viscosity μ, e.g.,

$$\mu_t = \mu + \rho\varepsilon_m \tag{2}$$

where ρ is the fluid density. The new variable μ_t replaces the variable μ in the boundary-layer equations. For numerical calculations, Kosecoff et al.[28] assumes that ε_m is in the form of

$$\varepsilon_m = \varepsilon_{max} \exp[\beta_1 (y/K)^2] \tag{3}$$

where β_1 = constant equal to 1.0

y = distance along the surface normal

K = distributed roughness height

ε_{max} = amplitude of the momentum diffusivity at the wall given by

$$\varepsilon_{max} = K_\varepsilon \nu R_K [1-\exp(-R_K/A+)] \tag{4}$$

The variables in Equation (4) are K_ε, a constant equal to 0.094; ν the kinematic viscosity of the fluid; R_K the roughness Reynolds number ($R_K=u_K K/\nu$, u_K the local streamwise velocity component evaluated at the roughness height K); and A^+ a threshhold roughness Reynolds number assumed to equal 40 (obviously, for $R_K<A^+$ the effects of roughness diminish exponentially).

A computer code has been developed at DTNSRDC to calculate: 1. the boundary-layer characteristics, 2. linear boundary-layer instability, and 3. the spatial amplification of disturbances in the boundary layers on the bodies with distributed roughness. Similar to the computer program coded by Merkle et al.,[29] the rough-wall viscosity μ_t modeled by Equations (2) through (4) replaces the smooth-wall viscosity μ in the boundary-layer equations. Standard numerical procedures for

solving the boundary-layer properties[30] and the spatial amplification factor[29,31] are employed and will not be given here. The distributed roughnesses used in the experiments are the irregular particles glued on the surfaces of the headforms. In the following calculations, the roughness height K is selected to be $3K_s$, where K_s is the measured rms value of the roughness heights. The roughness height K is about equal to the average value of the maximum individual roughness depth, which is the vertical distance between the highest and lowest points of the roughness profile within a single measuring length of 1 cm. For an isolated ring of roughness, the roughness Reynolds number $R_K = u_K K/\nu$ is also used, where u_K is the smooth laminar boundary-layer velocity at the leading edge of the roughness band evaluated at a height of K. The value of K is taken as the average vertical distance between the tip of the largest roughness and the smooth surface in a circumferential distance of 1 cm.

CORRELATION FOR THREE SMOOTH HEADFORMS

The critical Reynolds number, $R_{D_{crit}}$, at which laminar separation disappears as a result of the occurrence of natural flow transition at the separation point can be estimated by observing the disappearance of a band of oil-film following the separation location. As shown in Figure 3a, the band of oil-film was visible at lower tunnel speeds and disappeared at higher speeds. The measured value of $R_{D_{crit}}$ for the smooth Headform S-2, as shown in Table 4 correlates well with the computed spatial amplification factor $A_s = e^7$ at the separation location. The value of $R_{D_{crit}}$ for the smooth S-1 model occurs beyond the maximum speed capability of the 36-in. water tunnel.[1] Similar correlations between the measured values of $R_{D_{crit}}$ and the computed values of A_s are shown in Table 3 (Figure 6) and in Table 4 for Headforms S-1 and S-2, respectively, with distributed roughness. The measured values of $R_{D_{crit}}$ on the two headforms with distributed roughness correlate with the computed values of $A_s = e^7$ to e^9 for the five cases shown in Tables 3 and 4. Furthermore, the transition region on Headform T-6 as measured in a wind tunnel with low free-stream turbulence level[1,26] (about 0.1%) correlates well with the computed

spatial amplification factor of $A = e^{11}$ and the transition region on Headform T-6 in the 36-in. water tunnel with a higher turbulence level (about 0.45%) is likely to occur in a location where the computed values of A are less than e^{11}. The above correlations imply that the spatial amplification factor can be used as a simple yardstick to correlate transition on bodies with and without distributed roughness. In order to determine the minimum distributed roughness height necessary to trip the boundary layer, an arbitrary conservative estimate of $A = e^{13}$ is recommended. Flow transition is quite certain to occur at a location where the computed spatial amplification factor is equal to or less than e^{13}.

As shown in Tables 3, 4, and 5, the flow is laminar at the C_{pmin} location for every smooth headform. This conclusion is based on the estimated transition location which is considerably aft of the C_{pmin} location for the three bodies. At the laminar separation point of the smooth Headform S-1, the flow is still laminar at the highest test values of R_D investigated. Also, small band cavitation inception was observed with $\sigma_i \cong -C_{ps} < -C_{pmin}$ (Table 3 and Figure 2). The predicted transition location occurs a small distance downstream of the laminar separation location on the large (D=10.2 cm) smooth Headform S-2 at $R_D = 1.3 \times 10^6$, whereas transition is predicted at a small distance upstream of the separation at $R_D = 1.9 \times 10^6$. Large transient spot cavitation inception was observed on Headform S-2 with $\sigma_i \cong -C_{ps} < -C_{pmin}$ (Table 4 and Figure 3). For the range of $1.3 \leq R_D \times 10^{-6} \leq 1.9$, the laminar separation was found to be intermittent with a short separation bubble. On the small (D=2.54 cm) smooth Headform S-2 at $R_D \cong 4 \times .0^5$, the predicted transition location occurs a considerable distance downstream of the laminar separation point and a long separation bubble is predicted.[9] Attached patch cavitation inception was observed on the small Headform S-2 with $\sigma_i < -C_{ps}$ (Table 4 and Figure 3). Furthermore, the predicted transition locations shown in Table 4 are considerably aft of the C_{pmin} location. On smooth Headform T-6, the traveling-bubble cavitation inception with $-C_{ptr} > \sigma_i > -C_{pmin}$, was observed initially and then the attached patch cavitation inception, with $\sigma_i \cong -C_{ptr} < -C_{pmin}$ was observed in the transition region. The predicted transition locations occur a considerable distance downstream of the minimum pressure locations for all the three smooth headforms, and the measured incipient cavitation numbers are all significantly smaller than the values of $-C_{pmin}$.

CORRELATION FOR THREE HEADFORMS WITH DISTRIBUTED ROUGHNESS

The predicted transition locations on the three headforms with densely and loosely packed distributed roughness are given in Tables 3 through 5. For the two model sizes tested (D=10.2 and 2.54 cm), all the predicted transition locations occur a small distance from the stagnation point and a considerable distance upstream of the minimum pressure locations. Therefore, all the flows over the headforms with distributed roughness are definitely turbulent at the C_{pmin} locations for the Reynolds numbers tested. Under this condition, the measured cavitation inception numbers are found to be very close to the values of $-C_{pmin}$, e.g., $\sigma_i = -C_{pmin} \pm 0.02$. In each case, cavitation inception was observed to be in the form of attached small cavitation bubble lines evenly distributed around the location of the C_{pmin} (see Figures 6 and 7). These results suggest that the distributed roughness height should be selected so as to move the transition location forward of the location of minimum pressure. Other correlations, for the Schiebe Model tested by Billet and Holl[10] are given in the appendix.

CORRELATION FOR THREE HEADFORMS WITH ISOLATED ROUGHNESS BANDS

The measured cavitation inception indices for the headforms with isolated roughness bands located upstream of the C_{pmin} location are also presented in Tables 3 through 5. The width of the roughness band is small (< 4 mm). The computed roughness Reynolds numbers based on the roughness height K at the leading edge of the roughness band, $R_K = u_K K/\nu$, are also given in the tables, where u_K is the smooth laminar boundary-layer velocity at the band leading-edge evaluated at a height of K. As shown in Tables 3 through 5, the measured cavitation inception numbers for models with the roughness band approximate the values of $-C_{pmin}$ well when the computed values of R_K are equal to or greater than 600. However, when the computed values of R_K are less than 600, the measured values of σ_i are smaller than the computed value of $-C_{pmin}$. The incipient cavitation observed was attached patch type occurring near the C_{pmin} location. A minimum R_K value of 600 had been recommended to stimulate laminar boundary layers to turbulent flows by Preston[32] for circular wire trips and also by Braslow et al.[33] for sand trips. The same threshold value of R_K of 600 is required for the isolated roughness bands to

promote earlier transition and to simulate proper cavitation inception. Furthermore, the roughness bands must be located upstream of the minimum pressure location to assure a fully-developed turbulent boundary layer at C_{pmin}.

CONCLUSIONS

Cavitation inception observations were made in the DTNSRDC 36-in. water tunnel on three axisymmetric headforms with and without various turbulence stimulators. The experiments were designed to identify conditions under which the cavitation inception number could be approximated by the negative of the minimum pressure, $-C_{pmin}$. The following conclusions may be drawn.

For smooth models and models with distributed roughness, a correlation may exist between the transition location, the location and value of minimum pressure, and the cavitation inception number. For models with isolated roughness bands upstream of the negative pressure location, a correlation may be made between the roughness Reynolds number $R_K = u_K K/\nu$, the location and value of minimum pressure, and the cavitation inception number. Furthermore, analytical methods may be sufficient to predict the correlations. Computed spatial amplification factors, e^N ($7<N<10$), of laminar boundary layer disturbances were found in this investigation to predict reasonably well the measured flow transition on Headforms S-1 and S-2 with and without distributed roughness. Potential flow theory may be used to predict the minimum pressure value and location. Transition is predicted to occur considerably aft of $-C_{pmin}$ for the smooth models and the cavitation inception number was found to be much smaller than the value of the negative pressure coefficient. On the models with distributed roughness, transition occurred ahead of $-C_{pmin}$ and the cavitation number was approximately equal in value to the negative of the minimum pressure coefficient. Incipient cavitation numbers on the models with isolated roughness bands were found to approximate the computed values of $-C_{pmin}$ when the roughness Reynolds numbers were equal to or greater than 600.

The type of incipient cavitation may vary with the use of a turbulence stimulator. Incipient cavitation on the smooth models was observed as small band, transient spot, and traveling bubble or attached spot on Headforms S-1, S-2, or S-3, respectively. On the models with distributed roughness, incipient cavitation

occurred as attached small cavitating bubble lines evenly distributed about the minimum pressure location. Attached patch type cavitation was observed in the vicinity of the minimum pressure location for the headforms having the isolated roughness band.

In order to assure that the flow is fully turbulent at the minimum pressure location, a conservative computed spatial amplification factor A about equal to e^{13} is recommended when using distributed roughness as a turbulence stimulator. Excessively large distributed roughness heights which cause extremely large increases of A (i.e. $A>e^{20}$) should not be used. Furthermore, it is recommended that the roughness be distributed between the stagnation point and a location downstream of the minimum pressure location so that no surface discontinuity may be caused by the roughness. Under these conditions, the measured cavitation inception number σ_i can be expected to closely approximate the value of $-C_{pmin}$. When a threshold roughness Reynolds number R_K of 600 is satisfied for isolated turbulence stimulators located upstream of the minimum pressure location, the measured value of σ_i is also expected to closely approximate the value of $-C_{pmin}$.

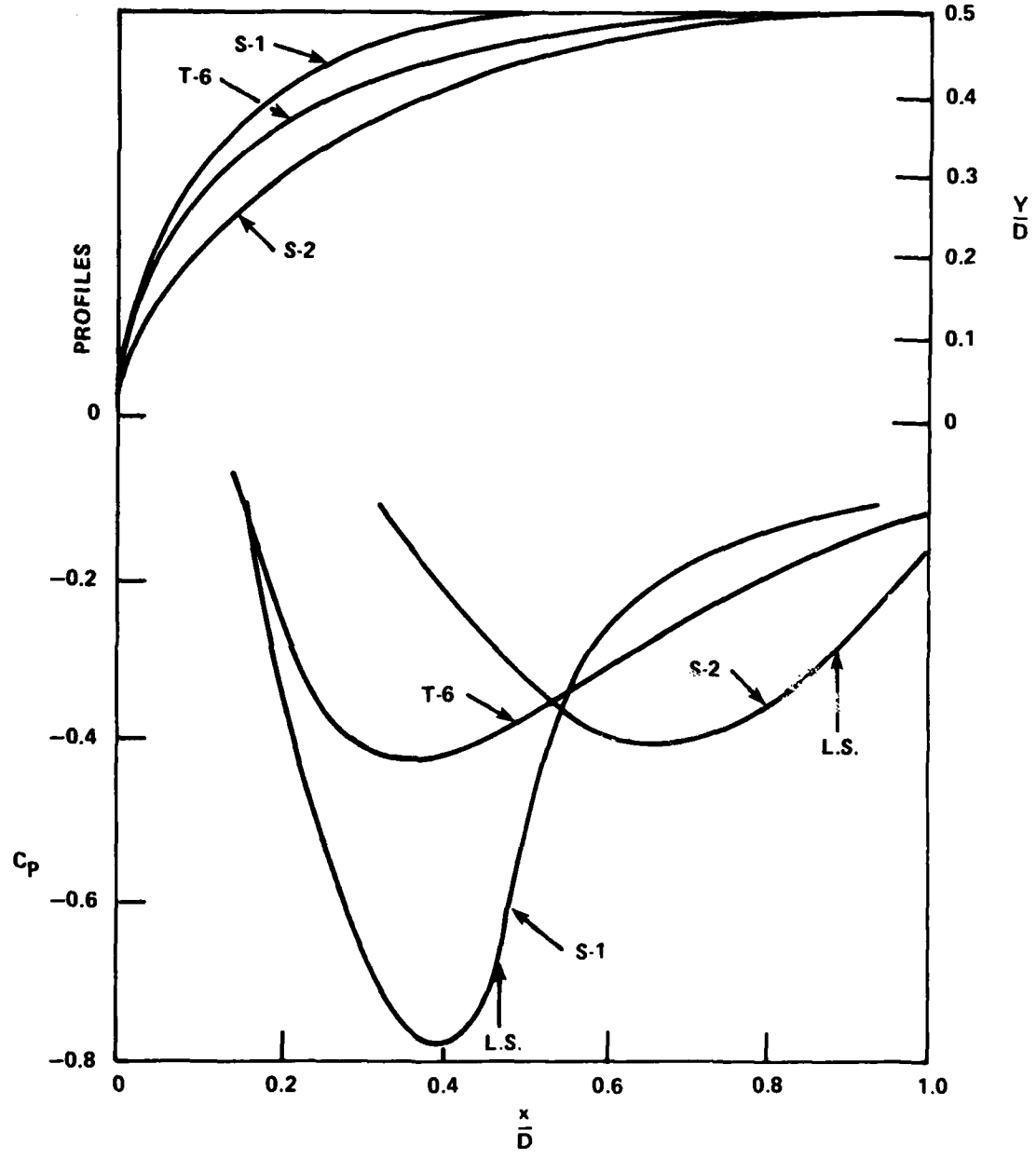

Figure 1 - Surface Profiles and Pressure Coefficients of Three Headforms

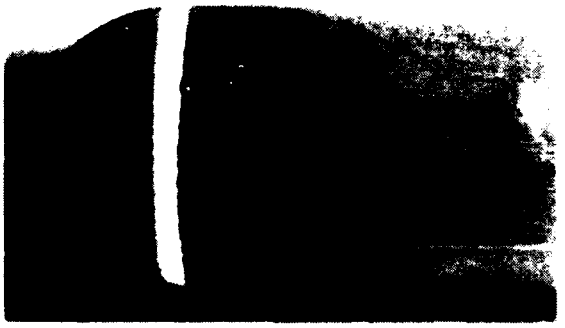

Figure 2a - Laminar Separation
Occurring at $(x/D)_S = 0.47$

Figure 2b - Attached Band Cavitation
with Small Bubble Lines Distributed
Evenly at Laminar Separation
(σ_i=0.61)

Figure 2 - Small Band Cavitation Inception Occurring at a Laminar Separation Location on the Smooth S-1 Headform

Figure 3a - A Small Laminar Separation Bubble at $(x/D)_S = 0.89$

Figure 3b - Cavitation Inception at $\sigma_i = 0.30$, D = 10.2 cm

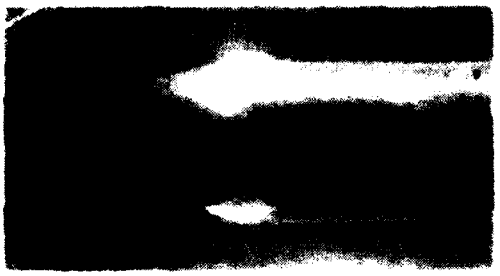

Figure 3c - Cavitation Inception at $\sigma_i = 0.30$, D = 7.63 cm

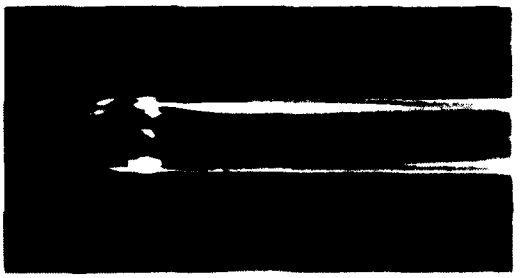

Figure 3d - Cavitation Inception at $\sigma_i = 0.23$, D = 2.54 cm

Figure 3 - Three Sizes of Large Transient Spots at Laminar Separation on Smooth S-2 Headforms

Figure 4a - Traveling Bubble at $\sigma_i = 0.33$

Figure 4b - Attached Patch at $\sigma_i = 0.23$

Figure 4 - Two Types of Cavitation Inception on the Smooth Headform T-6

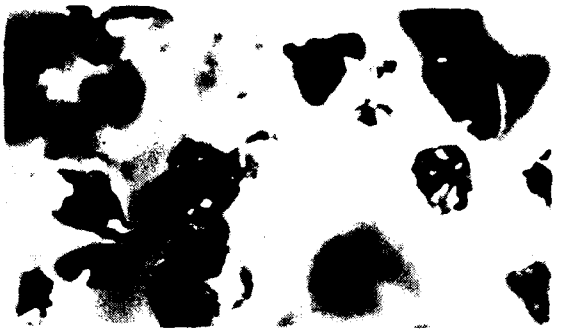

Figure 5a - Loosely Packed 60 μm Particles

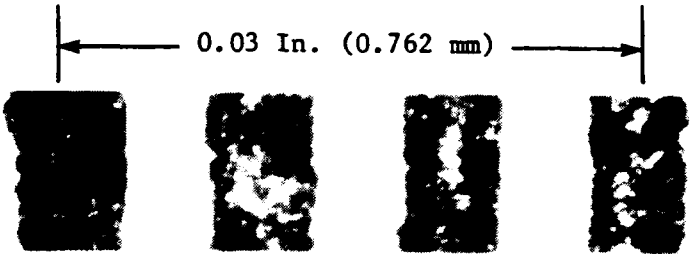

Figure 5b - 0.01-In. (254-μm) Scale

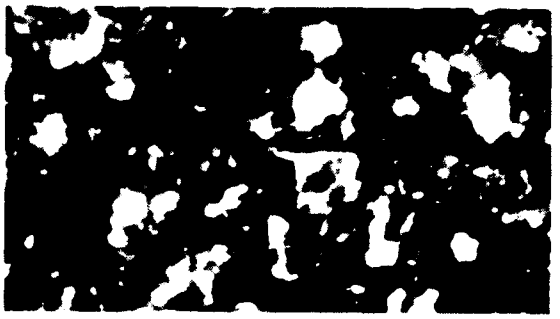

Figure 5c - Densely Packed 60 μm Particles

Figure 5 - Distributed Roughness (Amplified × 110)

Figure 6 - Cavitation Inception on Headform S-1 with Boundary-Layer Turbulence Stimulators

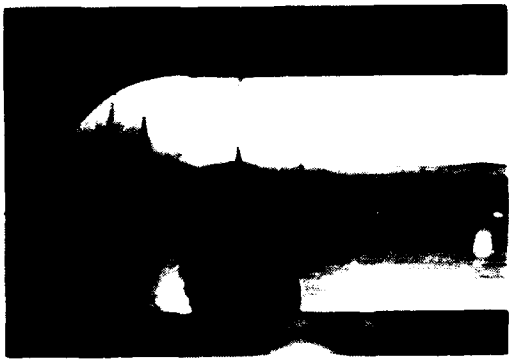

Figure 6a - $R_D = 3.2 \times 10^5$

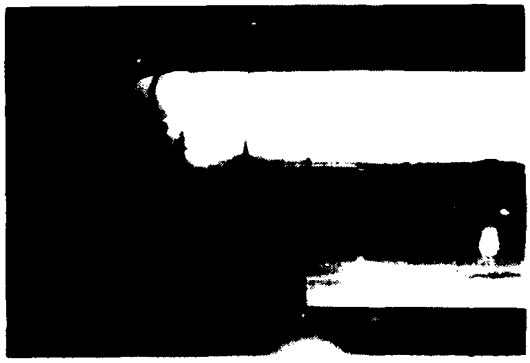

Figure 6b - $R_D = 5 \times 10^5$

(Both figures show loosely packed 60 μm particles on the upper half of the model and densely packed 60 μm particles on the lower half of the model.)

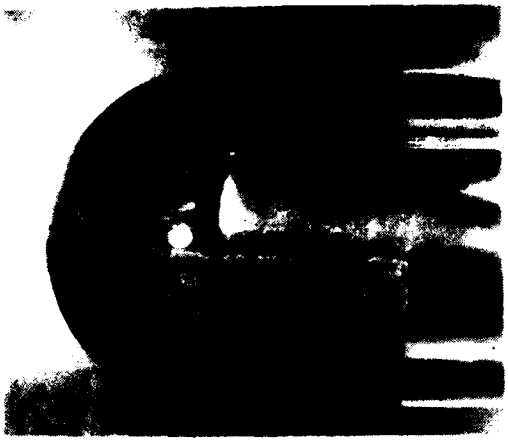

Figure 6c - Upper Half Cavitation Inception, $\sigma_i = 0.79$ at the C_{pmin} Location

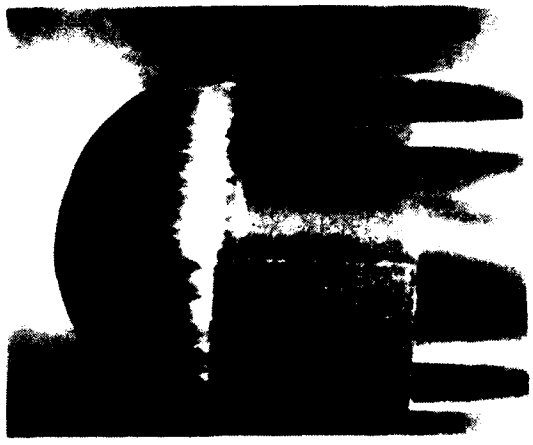

Figure 6d - Lower Half Cavitation Inception, $\sigma_i = 0.78$ at the C_{pmin} Location

Figure 6 (Continued)

Figure 6e - $R_D = 3.2 \times 10^5$

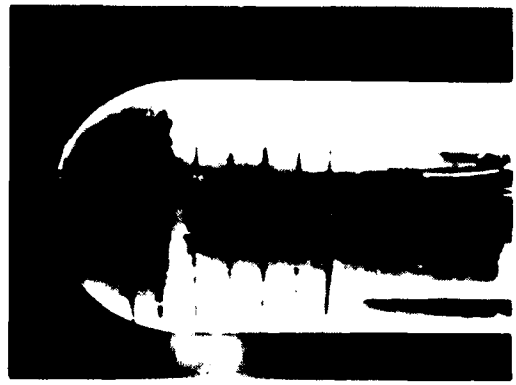

Figure 6f - $R_D = 5.7 \times 10^5$

(Both figures show a boundary-layer tripping band (2.5-mm wide and 0.03-mm high) located at x/D = 0.15 (C_p=0) of the upper half of the model and loosely packed 60 μm particles on the lower half.)

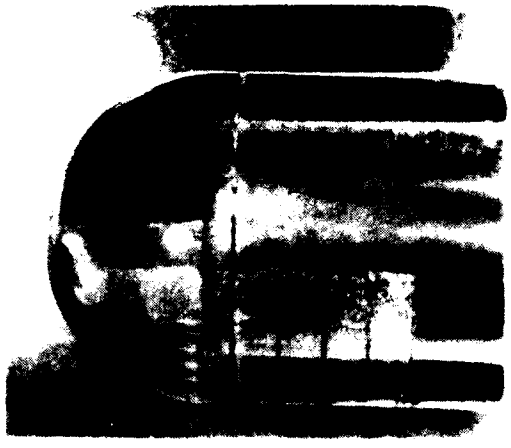

Figure 6g - Cavitation Inception at $\sigma_i = 0.78$ at the C_{pmin} of the Lower Half

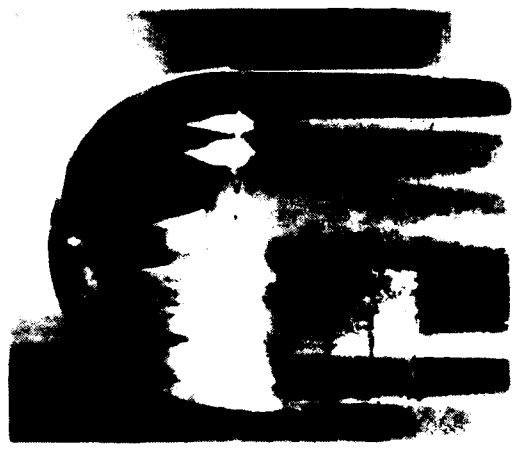

Figure 6h - Cavitation Inception at $\sigma_i = 0.70$ at the C_{pmin} of the Upper Half

Figure 6 (Continued)

Figure 6i - Cavitation Inception (σ_i=0.70)
at the C_{pmin} of the Headform with a
Boundary-Layer Tripping Band
(2.5-mm wide and 0.03-mm high)
Located at x/D = 0.2
(C_p=-0.33)

Figure 7a - Cavitation Inception (σ_i=0.42) on Both Halves of the Headform (D=10.2 cm), with Densely Packed 60 μm Particles on the Lower Half of the Model and a Tripping Band (4-mm wide and 0.06-mm high) at x/D = 0.125 (C_p=0.2) on the Upper Half

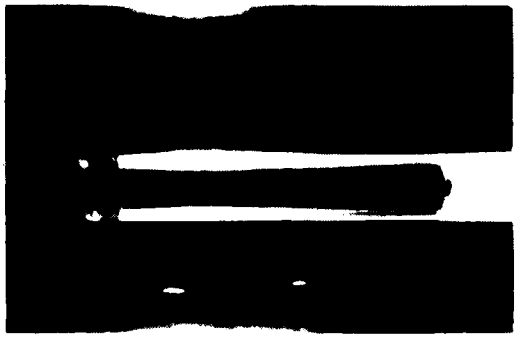

Figure 7b - Cavitation Inception (σ_i=0.42) on the Small (D=2.54 cm) Headform with Densely Packed 60 μm Particles

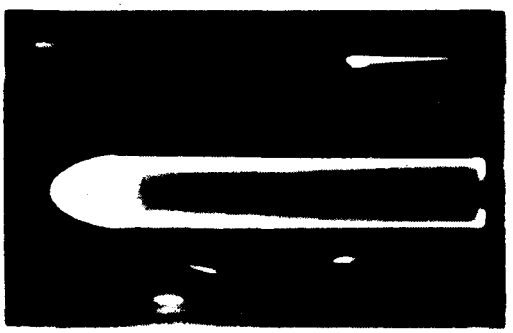

Figure 7c - Cavitation Inception (σ_i=0.42) on the Small (D=2.54 cm) Headform with Evenly Packed 90 μm Spherical Glass Beads

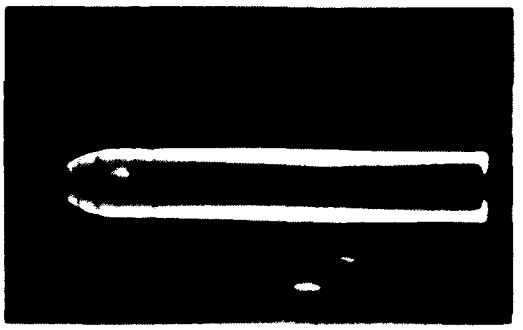

Figure 7d - Cavitation Inception (σ_i=0.38) on the Small (D=2.54 cm) Headform with a Tripping Band (1.3-mm wide and 0.04-mm high) at x/D = 0.25 (C_p=0.05)

Figure 7 - Cavitation Inception on Headform S-2 with Boundary-Layer Turbulence Stimulators

TABLE 1 - MEASURED CAVITATION INCEPTION ON SMOOTH HEADFORMS WITH LAMINAR SEPARATION

	Headform (Hemispheric Nose) S-1	Headform S-2	
Predicted[18] $R_D \times 10^6$ by e^7	5.0	1.3	
Predicted[18] $R_D \times 10^6$ by e^9	7.0	1.9	
Predicted[18] $R_D \times 10^6$ by e^{11}	9.0	2.5	
Measured $R_{D_{crit}} \times 10^6$	> 1.8 (36-in. Water Tunnel) > 2.5 (Wind Tunnel)	1.3 (36-in. Water Tunnel) 2.4 (Wind Tunnel)	
$-C_{pmin}$	0.78	0.41	
(x/D) at C_{pmin}	0.39	0.68	
$-C_{ps}$	0.63	0.30	
$(x/D)_s$	0.47	0.89	
$(S/D)_s$	0.76	1.10	
Measured σ_i	$\sigma_i = 0.61 \pm 0.02$ $0.7 < R_D \times 10^{-6} < 1.9$	D = 7.63 cm & 10.2 cm $\sigma_i = 0.30 \pm 0.02$ $1.2 < R_D \times 10^{-6} < 1.8$	D = 2.54 cm $\sigma_i = 0.23 \pm 0.02$ $0.3 < R_D \times 10^{-6} < 0.5$
σ_i versus $-C_{ps}$	$\sigma_i \cong -C_{ps}$	$\sigma_i = -C_{ps}$	$\sigma_i < -C_{ps}$
Incipient cavitation type for $R_D < R_{D_{crit}}$	Attached band cavitation with small bubble lines distributed evenly at laminar separation	Large transient attached cavitating spots (fingers) at laminar separation	
α/α_o	0.40	0.40	
α/α_{TS}	0.5~2.1	0.8~3.0	

TABLE 2 - MEASURED CAVITATION INCEPTION ON SMOOTH HEADFORM T-6 WITH NATURAL TRANSITION

$R_D = 1.3 \times 10^6$			α/α_o	α/α_{TS}	σ_i	Type of Cavitation
Estimated Transition						
A	x/D	$-C_{ptr}$				
e^7	0.62	0.30	0.40	1.6	0.33 ± 0.03	Traveling Bubble
e^9	0.68	0.26		2.1	0.23 ± 0.02	Attached Patch
e^{11}	0.72	0.24				
e^{13}	0.83	0.23				
$R_D = 1.9 \times 10^6$			α/α_o	α/α_{TS}	σ_i	Type of Cavitation
Estimated Transition						
A	x/D	$-C_{ptr}$				
e^7	0.59	0.31	0.40	1.0	0.33 ± 0.03	Traveling Bubble
e^9	0.64	0.28		1.7	0.23 ± 0.02	Attached Patch
e^{11}	0.69	0.26				
e^{13}	0.75	0.26				
$C_{pmin} = 0.43$ at x/D = 0.37						

TABLE 3 - MEASURED CAVITATION INCEPTION ON HEADFORM S-1 HAVING VARIOUS BOUNDARY-LAYER TURBULENCE STIMULATORS

	Smooth (rms Finish < 0.4 μm)	Densely Packed 60 μm Distributed Roughness	Loosely Packed 60 μm Distributed Roughness	Boundary-Layer Tripping Band (2.5-mm wide and 0.03-mm high) Located at either x/D = 0.15 or 0.20
$R_D = 1.3 \times 10^6$	$X_{tr}/D > 0.47$ $\sigma_i = 0.61 \pm 0.02$ Attached ring of small cavitating bubbles at laminar separation (Figure 2)	$X_{tr}/D < 0.6$ $\sigma_i = 0.77 \pm 0.01$* (Figure 6d)	$X_{tr}/D < 0.09$ $\sigma_i = 0.78 \pm 0.01$* (Figure 6c)	$\frac{u_K K}{\nu} = 190$ and 210 $\sigma_i = 0.70 \pm 0.03$ Attached large spot cavitation (Figures 6g and 6h)
$R_D = 1.9 \times 10^6$	$X_{tr}/D > 0.47$ $\sigma_i = 0.61 \pm 0.02$ Attached ring of small cavitating bubbles at laminar separation	$X_{tr}/D < 0.04$ $\sigma_i = 0.78 \pm 0.01$*	$X_{tr}/D < 0.04$ $\sigma_i = 0.79 \pm 0.01$*	$\frac{u_K K}{\nu} = 330$ and 360 $\sigma_i = 0.70 \pm 0.02$ Attached large spot cavitation
Measured $R_{D_{crit}}$	$> 1.9 \times 10^6$	$\simeq 3.6 \times 10^5$ at the computed location of $A_s = e^9$ at laminar separation (K=45 μm)	$\simeq 5.4 \times 10^5$ at the computed location of $A_s = e^8$ at laminar separation (K=30 μm)	$\simeq 5.7 \times 10^5$

NOTE: D = 10.2 cm, $C_{pmin} = -0.78$ at x/D = 0.39, $C_{ps} = -0.63$ at $X_s/D = 0.47$

X_{tr} = estimated transition location using $A = e^{13}$.

*Observed cavitation inception with attached small cavitating bubble lines distributed around C_{pmin}.

TABLE 4 - MEASURED CAVITATION INCEPTION ON HEADFORM S-2 HAVING VARIOUS BOUNDARY-LAYER TURBULENCE STIMULATORS

	Turbulence Stimulators		
	Smooth (rms Finish < 0.4 μm)	Densely Packed 60 μm Distributed Roughness	*Boundary-Layer Tripping Band* (4-mm wide and 0.06-mm high) Located at x/D = 0.125
$R_D = 1.3 \times 10^6$	$X_{tr}/D \geq 0.89$ $\sigma_i = 0.30 \pm 0.02$ Large transient attached cavitating spots (fingers) at laminar separation (Figures 3a and 3b)	$X_{tr}/D < 0.07$ $\sigma_i = 0.42 \pm 0.01$* (Figure 7a)	$\frac{u_K K}{\nu} = 520$ $\sigma_i = 0.42 \pm 0.01$ Attached cavitating spots at the C_{pmin} location (Figure 7a)
$R_D = 1.9 \times 10^6$	$X_{tr}/D < 0.899$ $\sigma_i = 0.30 \pm 0.02$ Large transient attached cavitating spots (fingers) off and on at laminar separation	$X_{tr}/D < 0.04$ $\sigma_i = 0.42 \pm 0.01$*	$\frac{u_K K}{\nu} = 870$ $\sigma_i = 0.42 \pm 0.01$ Attached cavitating spots at the C_{pmin} location
Measured $R_{D_{crit}}$	$\geq 1.3 \times 10^6$ at the computed location of $A_s = e^7$ at laminar separation	$\approx 4.0 \times 10^5$ at the computed location of $A_s = e^7$ at laminar separation (K=45 μm)	$\approx 3.2 \times 10^5$

NOTE: D = 10.2 cm, $C_{pmin} = -0.41$ at x/D = 0.68, $C_{ps} = -0.30$ at x/D = 0.89

X_{tr} = estimated transition location by using $A = e^{13}$.

*Observed cavitation inception with attached small cavitating bubble lines evenly distributed around C_{pmin}.

TABLE 4 (Continued)

	Turbulence Stimulators			
	Smooth (rms Finish < 0.4 μm)	Densely Packed 60 μm Distributed Roughness	Densely and Evenly Packed 90-μm Spherical Glass Beads	Boundary-Layer Tripping Band (1.3-mm wide and 0.05-mm high) Located at x/D = 0.25
$R_D = 4 \times 10^5$	$X_{tr}/D > 0.89$ $\sigma_i = 0.23 \pm 0.02$ Large attached patch cavitation at laminar separation (Figure 3d)	$X_{tr}/D < 0.13$ $\sigma_i = 0.42 \pm 0.01$* (Figure 7b)	$X_{tr}/D < 0.13$ $\sigma_i = 0.41 \pm 0.01$* (Figure 7c)	$\frac{u_K K}{\nu} = 520$ $\sigma_i = 0.38 \pm 0.02$ Large attached cavitating spots around C_{pmin} (Figure 7d)
Measured $R_{D_{crit}}$		$\simeq 1.0 \times 10^5$ at the computed location of $A_s = e^7$ at laminar separation (K=35 μm)	$\simeq 0.9 \times 10^5$ at the computed location of $A_s = e^8$ at laminar separation (K=45 μm)	$\simeq 1.1 \times 10^5$

NOTE: D = 2.54 cm, $C_{pmin} = -0.41$ at x/D = 0.68, $C_{ps} = -0.30$ at $X_s/D = 0.89$

X_{tr} = estimated transition location by using $A = e^{13}$.

*Observed cavitation inception with attached small cavitation bubble lines evenly distributed around C_{pmin}.

TABLE 5 - MEASURED CAVITATION INCEPTION ON HEADFORM T-6 HAVING VARIOUS BOUNDARY-LAYER TURBULENCE STIMULATORS

	Turbulence Stimulators		
	Smooth (rms Finish < 0.4 μm)	Densely Packed 60 μm Distributed Roughness	Boundary-Layer Tripping Band (2.54-mm wide and 0.03-mm high) Located at x/D = 0.125
$R_D = 1.3 \times 10^6$	Estimated Transition, ($e^7 \sim e^{13}$) $0.62 < X_{tr}/D < 0.83$ $\sigma_i = 0.33 \pm 0.03$ (Figure 4a) Traveling-bubble cavitation $\sigma_i = 0.23 \pm 0.02$ (Figure 4b) Attached cavitating patches	Estimated Transition, (e^{13}) $X_{tr} < 0.06$ $\sigma_i = 0.42 \pm 0.01$*	$\frac{u_K K}{\nu} = 200$ $\sigma_i = 0.35 \pm 0.02$ Large attached cavitating patches
$R_D = 1.9 \times 10^6$	$0.60 < X_{tr}/D < 0.75$ $\sigma_i = 0.33 \pm 0.03$ Traveling-bubble cavitation $\sigma_i = 0.23 \pm 0.02$ Attached cavitating patches	$X_{tr}/D < 0.04$ $\sigma_i = 0.42 \pm 0.01$*	$\frac{u_K K}{\nu} = 340$ $\sigma_i = 0.37 \pm 0.02$ Large attached cavitating patches

NOTE: D = 10.2 cm, $C_{pmin} = 0.43$ at x/D = 0.37

X_{tr} = Estimated transition location by using $e^7 \sim e^{13}$ for smooth surface and e^{13} for distributed roughness.

*Observed cavitation inception with attached small cavitating bubble lines evenly distributed around C_{pmin}.

APPENDIX

CORRELATION FOR SCHIEBE MODEL

Transition predictions for a Schiebe model ($-C_{pmin}$=0.75) with and without distributed roughness corresponding to the experiments conducted by Billet and Holl[10] are shown in Table 6. The roughness was distributed in the forward region of the model starting from the stagnation point and extending aft to a local diameter D_r, which is upstream of the C_{pmin} location. As shown in Table 6, the computed spatial amplification factors for D_r/D = 0.5 and K = 60 μm are less than e^7 for the entire range of Reynolds numbers tested. Thus, the forward roughness extending to D_r/D = 0.5 was not sufficient to trip the boundary layer, and cavitation inception was found[10] to be unaffected by this extent of distributed roughness. It is most likely that the distributed roughness of D_r/D = 0.7 and K = 30 μm has effectively tripped the boundary layer for the case $R_D = 8 \times 10^5$ since the computed value of A in this case is greater than e^{13}. For $4.5 \times 10^5 \leq 8 \times 10^5$, the distributed roughness extending to D_r/D = 0.7 is predicted to have a significant influence on the boundary-layer transition location $A > e^7$ when compared with smooth surface data (A are all less than e^0 at the C_{pmin} location). Significant differences in the observed cavitation inception results were found[10] between the smooth body and the body with this distributed roughness on the model with a diameter of D = 50.8 mm. For the smaller body, the computed values of A are all less than e^7. However, the differences in the observed cavitation inception with and without the same distributed roughness were found to be much smaller on the body with D = 25.4 mm and $R_D < 4.5 \times 10^5$. The observed differences in cavitation inception with and without distributed roughness on the Schiebe model tested by Billet and Holl[10] are generally in agreement with the predicted differences in transition.

TABLE 6 - TRANSITION PREDICTIONS FOR SCHIEBE MODEL ($-C_{pmin}$=0.75) WITH AND WITHOUT DISTRIBUTED ROUGHNESS

Model Diameter (mm)	Reynolds Number $R_D \times 10^{-5}$	Computed Values of A				
		At D_r/D = 0.5		At D_r/D = 0.7		At C_{pmin}
		K = 0	K = 60 μm	K = 0	K = 30 μm	K = 0
25.4	3.1	$e^{<0}$	$e^{2.3}$	$e^{<0}$	$e^{4.5}$	$e^{<0}$
	4.5	$e^{<0}$	$e^{4.1}$	$e^{<0}$	$e^{5.8}$	$e^{<0}$
50.8	4.5	$e^{<0}$	$e^{3.3}$	$e^{<0}$	$e^{9.6}$	$e^{<0}$
	8.0	$e^{<0}$	$e^{6.0}$	$e^{<0}$	$e^{>13}$	$e^{<0}$
203.2	20.0	-	-	-	-	$e^{<0}$
	40.0	-	-	-	-	$e^{\simeq 0}$

REFERENCES

1. Huang, T.T., "Cavitation Inception Observations on Six Axisymmetric Headforms," Journal of Fluids Engineering, American Society of Mechanical Engineers, Vol. 103, No. 2, pp. 273-278 (Jun 1981).

2. Arakeri, V.H. and A.J. Acosta, "Cavitation Inception Observations on Axisymmetric Bodies at Supercritical Reynolds Numbers," Journal of Ship Research, Vol. 20, No. 1, pp. 40-50 (1976).

3. Holl, J.W. and J.A. Carroll, "Observations of the Various Types of Limited Cavitation On Axisymmetric Bodies," Journal of Fluids Engineering, American Society of Mechanical Engineers, Vol. 103, No. 3, pp. 415-423 (Sep 1981).

4. Van der Meulen, J.H.J., "Boundary Layer and Cavitation Studies of NACA-16-012 and NACA 4412 Hydrofoils," Proc. 13th Symposium on Naval Hydrodynamics, Tokyo, Japan, Oct 6-10, 1980, published by Shipbuilding Research Association of Japan, pp. 195-217 (1981).

5. Van der Meulen, J.H.J. and Yuan-Pei Ye, "Cavitation Inception Scaling by Roughness and Nuclei Generation," paper presented at the 14th Symposium on Naval Hydrodynamics, Ann Arbor, Michigan (Aug 23-27, 1982).

6. Acosta, A.J. and B.R. Parkin, "Cavitation Inception - A Selective Review," Journal of Ship Research, Vol. 19, No. 4, pp. 193-205 (1975).

7. Acosta, A.J. and B.R. Parkin, "Report of the ATTC Cavitation Inception Committee," Proc. 19th ATTC, Ann Arbor, Michigan (Jul 1981).

8. Acosta, A.J., "Cavitation Inception and Internal Flows with Cavitation," The Fourth David W. Taylor Lecture, Report DTNSRDC-79/011 (Oct 1979).

9. Huang, T.T. and F.B. Peterson, "Influence of Viscous Effects on Model Full-Scale Cavitation Scaling," Journal of Ship Research, Vol. 20, No. 4, pp. 215-223 (1976).

10. Billet, M.L. and J.W. Holl, "Scale Effects on Various Types of Limited Cavitation," Journal of Fluids Engineering, Vol. 103, No. 3, pp. 405-414 (Sep 1981).

11. Albrecht, K. and Bjorheden, "Cavitating Testing of Propellers in a Free Surface Tunnel Utilizing Micro Air Bubble Control," Journal of Fluids Engineering, American Society of Mechanical Engineers, Vol. 97, pp. 523-532 (1975).

12. Noordzij, L., "Some Experiments on Cavitation Inception with Propellers in the NSMB - Depressurized Towing Tank," International Shipbuilding Progress, Vol. 23, No. 265, pp. 300-306 (1976).

13. Gates, E.M. and A.J. Acosta, "Some Effects of Several Freestream Factors on Cavitation Inception on Axisymmetric Bodies," paper presented at the 12th Symposium on Naval Hydrodynamics, Wash., D.C., June 5-9, 1978, published by National Academy of Sciences, Wash., D.C., pp. 86-110 (1979).

14. Ling, S.C. et al., "Inception of Cavitation Over Headforms and Hydrofoils," paper presented at the 14th Symposium on Naval Hydrodynamics, Ann Arbor, Michigan, (Aug 23-27, 1982).

15. Kuiper, G., "Scale Effects on Propeller Cavitation Inception," paper presented at the 12th Symposium on Naval Hydrodynamics, Wash., D.C., June 5-9, 1978, published by National Academy of Sciences, Wash., D.C., pp. 401-429 (1979).

16. Kuiper, G., "Cavitation Inception on Ship Propeller Models, " Ph.D Thesis Delft, Netherlands (1981).

17. Kuiper, G., "Some Experiments with Specific Types of Cavitation on Ship Propellers," Journal of Fluids Engineering, American Society of Mechanical Engineers, Vol. 104, No. 1, pp. 105-114 (Mar 1982).

18. Kuiper, G., "A Comparison Between Cavitation Inception Phenomena in a Cavitation Tunnel and in a Depressurized Towing Tank," The Royal Institute of Naval Architects Spring Meeting, Paper No. 5 (1982).

19. Billet, M.L. and J.W. Holl, "The Use of Distributed Roughness for Scaling Cavitation Inception," Proc. 19th ATTC, Ann Arbor, Michigan, pp. 971-988 (Jul 9-11, 1980).

20. Shen, Y.T. and R. Eppler, "Wing Sections for Hydrofoils - Part 2: Nonsymmetrical Profiles," Journal of Ship Research, Vol. 25, pp. 39-45 (Sep 1981).

21. Shen, Y.T., "Cavitation-Free Buckets of YS-920 and NACA 66 (MOD) Foil Section," Report DTNSRDC/SPD-1049-01 (Jul 1982).

22. Arakeri, V.H. and A.J. Acosta, "Viscous Effects in the Inception of Cavitation on Axisymmetric Bodies," Journal of Fluids Engineering, American Society of Mechanical Engineers, Vol. 96, No. 4, pp. 519-527 (Dec 1973).

23. Smith, A.M.O., "Transition, Pressure Gradient, and Stability Theory," Proceedings of the Ninth International Congress of Applied Mechanics, Brussels, Belgium, Vol. 4, pp. 234-243 (1957).

24. Arakeri, V.H., "A Note of Transition Observation on an Axisymmetric Body and Some Related Fluctuating Wall Pressure Measurements," Journal of Fluids Engineering, American Society of Mechanical Engineers, Vol. 97, No. 1, pp. 82-87 (1975).

25. Huang, T.T. and D.E. Hannan, "Pressure Fluctuations in the Regions of Flow Transition," NSRDC Report 4723 (1975).

26. Huang, T.T., "Pressure Fluctuations in the Transition Regions of Forebodies of Revolution," Proceedings of Low-Speed Boundary-Layer Transition Workshop II, The Rand Corporation P-6119 (Edited by W.S. King and M. Kokata) (1978).

27. Power, J.L., "Drag, Flow Transition, and Laminar Separation on Nine Bodies of Revolution Having Different Forebody Shapes," DTNSRDC Report 77-0065 (1977).

28. Kosecoff, M.A. et al., "An Analytical Study of the Effect of Surface Roughness on the Stability of a Heated Water Boundary Layer," Physical Dynamics, Inc., PDT-76-131 (1976).

29. Merkle, C.L. et al., "An Analytical Study of the Effect of Surface Roughness on Boundary-Layer Stability," Dynamics Technology, Inc., Report DT-7606-4 (1977).

30. Cebeci, T. and A.M.O. Smith, "Analysis of Turbulent Boundary Layers," Academic Press, New York (1974).

31. Okamura, T.T., "A Method for Calculating Laminar Boundary-Layer Profiles and Their Spatial Stability Properties for Two-Dimensional and Axisymmetric Bodies," Douglas Aircraft Company, Report MDC-J0097 (Dec 1971).

32. Preston, J.H., "The Minimum Reynolds Number for a Turbulent Boundary Layer and the Selection of a Transition Device," Journal of Fluid Mechanics, Vol. 3, Part 4, pp. 373-384 (1958).

33. Braslow, A.L. et al., "Use of Grit-Type Boundary-Layer Transition Trips on Wind-Tunnel Models," National Aeronautics and Space Administration, Report TN D-3579 (1966).

INITIAL DISTRIBUTION

Copies	
1	WES
1	U.S. ARMY TRAS R&D Marine Trans Div
1	CHONR/432 C.M. Lee
2	NRL 1 Code 2027 1 Code 2629
1	NORDA
3	USNA 1 Tech Lib 1 Nav. Sys. Eng. Dept. 1 B. Johnson
3	NAVPGSCOL 1 Lib 1 T. Sarpkaya 1 J. Miller
1	NADC
1	NOSC/Lib
1	NSWC, White Oak/Lib
1	NSWC, Dahlgren/Lib
1	NUSC/Lib
9	NAVSEA 1 05R24 (J. Sejd) 1 55W (R. Keane, Jr.) 1 55W3 (W. Sandberg) 1 50151 (C. Kennell) 1 56X1 (F. Welling) 1 56XP (F. Peterson) 1 63R31 (T. Peirce) 1 55N2 (A. Paladino) 1 99612 (Library)

Copies	
12	DTIC
1	AFOSR/NAM
1	AFFOL/FYS, J. Olsen
2	MARAD 1 Div of Ship R&D 1 Lib
1	NASA/HQ/Lib
1	NASA/Ames Res Ctr, Lib
2	NASA/Langley Res Ctr 1 Lib 1 D. Bushnell
3	NBS 1 Lib 1 P.S. Klebanoff 1 G. Kulin
1	NSF/Eng Lib
1	DOT/Lib TAD-491.1
2	MMA 1 National Maritime Research Center 1 Lib
1	Library of Congress/Science & Technology Div.
4	U of Cal/Dept Naval Arch, Berkley 1 Lib 1 W. Webster 1 J. Paulling 1 J. Wehausen
3	CIT 1 Aero Lib 1 T.Y. Wu 1 A.J. Acosta
1	Colorado State U/Eng Res Cen

Copies	
1	Cornell U/Shen
2	Harvard U 1 G. Carrier 1 Gordon McKay Lib
4	U of Iowa 1 Lib 1 L. Landweber 1 J. Kennedy 1 V.C. Patel
4	MIT 1 Lib 1 J.R. Kerwin 1 P. Leehey 1 J.N. Newman
2	U of Minn/St. Anthony Falls 1 Lib 1 R. Arndt
3	U of Mich/NAME 1 Lib 1 M. Parsons 1 F.G. Hammit
3	Penn State/ARL 1 B.R. Parkin 1 R.E. Henderson 1 ARL Lib
1	Princeton U/Mellor
1	U of Rhode Island 1 F.M. White
1	Science Application, Inc. Annapolis, MD C. von Kerczek
2	SIT 1 Lib 1 Breslin

Copies	
3	Stanford U 1 Eng Lib 1 R. Street, Dept Civil Eng 1 S.J. Kline, Dept Mech Eng
1	U of VA/Aero Eng Dept
1	VPI 1 J. Schetz, Dept Aero & Ocean Eng
3	Webb Inst 1 Lib 1 Lewis 1 Ward
1	SNAME/Tech Lib
1	Bell Aerospace
2	Boeing Company/Seattle 1 Marine System 1 P. Rubbert
1	Bolt, Beranek & Newman/Lib
1	Exxon, NY/Design Div Tank Dept
1	Exxon Math & System, Inc.
1	General Dynamics, EB/Boatwright
1	Flow Research
1	Gibbs & Cox/Tech Info
1	Grumman Aerospace Corp/Lib
4	Hydronautics 1 Lib 1 E. Miller 1 V. Johnson 1 C.C. Hsu

Copies	
1	Lockheed, Sunnyvale/Waid
2	McDonnell Douglas, Long Beach 1 T. Cebeci 1 J. Hess
1	Northrop Corp/Aircraft Div
1	Sun Shipbuilding/Chief Naval Arch
1	United Technology/East Hartford, Conn.
1	Westinghouse Electric

CENTER DISTRIBUTION

Copies	Code	Name
1	012.2	B.V. Nakonechny
1	15	W.B. Morgan
1	152	W.C. Lin
1	1521	W. Day
1	1522	G. Dobay
1	1522	M. Wilson
1	154	J. McCarthy
1	1540.1	R. Cumming
1	1540.2	B. Yim
30	1542	R. Cumming
1	1543	G. Santore
1	1544	T. Brockett
1	1544	R. Boswell
1	156	D. Cieslowski
1	156	G. Cox
1	1562	D. Moran
1	1564	J. Feldman
1	1606	T.C. Tai
1	184	J. Schot
1	1843	H. Haussling
1	19	M.M. Sevik
1	194	J.T. Shen
1	1942	F. Archibald
10	5211.1	Reports Distribution
1	522.1	Unclassified Lib (C)
1	522.2	Unclassified Lib (A)


FILM